Prediction of Visual Quality Metrics in Lossy Image Compression

S. Krivenko, F. Li, V. Lukin
Dept of Information-Communication Technologies
National Aerospace University – KhAI
Kharkiv, Ukraine
lukin@ai.kharkov.ua

B. Vozel
IETR UMR CNRS 6164, 22305
University of Rennes,
Lannion Cedex, France
benoit.vozel@univ-rennes1.fr

O. Krylova
Dept of Therapeutic Dentistry
Kharkiv National Medical University,
Kharkiv, Ukraine
krylovaol@ukr.net

***Abstract*— Images of different origin are widely used nowadays in various applications including medical diagnostic systems, remote sensing, etc. Due to modern tendency to improve imaging system resolution and increase image size, it has often become necessary to compress images before their storage and transferring via communication lines. Lossy compression is mostly employed for this purpose and an important task for it is to find and provide an appropriate compromise between compression ratio and quality of compressed data, in the first order, image visual quality. This paper considers an approach to predicting visual quality characterized by the metrics MSEHVSM or, equivalently, PSNR-HVS-M for the coder AGU based on discrete cosine transform (DCT). It is demonstrated that it is possible to estimate MSEHVSM in a limited number of 8x8 pixel blocks and then to predict this metric for the entire image for the considered coder. The influence of image content and the number of analyzed blocks is studied. It is shown that 500 or 1000 blocks are usually enough to carry out prediction with appropriate accuracy.**

Keywords— lossy compression; image; metric prediction; visual quality

I. INTRODUCTION

Images have become a part of our life and they are widely used for numerous applications in medicine [1], remote sensing [2], nondestructive control, etc. Each day a huge amount of images is acquired, transferred, and stored including images transferred via telecommunication channels in telemedicine [3]. Average size of acquired images increases, a typical size is nowadays hundreds of kB or even more than 1 MB [3]. Then, one can run into problems of image storage (available memory might be limited) and transferring (communication lines usually have a limited bandwidth; besides, an available time of data transferring can be limited as well). Therefore, it is desired to have intelligent and efficient methods for image compression [4].

Lossless (reversible) compression was thought to be the only possible for medical images about twenty tears ago [5]. The basic statement behind this was that no losses or distortions could be introduced by compression because important (diagnostic) information could not be lost. The main shortcoming of this approach is that the produced compression ratio (CR) is too small, commonly less that 3:1. Thus, lossy (irreversible) compression can be tried under conditions that valuable information is preserved [4, 5]. To determine the limits of acceptable losses, intensive studies have been performed [2, 6]. It happened so that acceptable CR depends upon the type of medical images and their peculiarities (complexity, noisiness. dimensionality). The authors of [6] consider acceptable even such large CR values as 40:1 for JPEG and 50:1 for JPEG2000. For other types of medical images, more "careful" recommendations concerning CR are given.

Experience collected by researchers in different applications of lossy image compression shows the following. First, compression performance depends upon image complexity that can be hardly characterized quantitatively but can be described verbally. A simple structure images are those ones that contain large homogeneous or quasi-homogeneous areas without high-contrast small-sized objects (details). In turn, there are complex structure images that contain a lot of details and/or textures. Simple structure images can be compressed with smaller distortions (for a given CR) or with a larger CR (for given losses characterized by mean square error (MSE) or peak signal-to-noise ratio (PSNR)) [7, 8]. Second, compression performance depends upon image dimension. RGB or multichannel images are compressed better since inter-channel correlation can be exploited [2]. Third, noise presence (its intensity) affects compression performance as well [9]. On one hand, noise presence leads to worse CR for the same losses. On the other hand, in lossy compression of noisy images, specific effect of partial noise removal is observed. Because of this, lossy compression of noisy images has to be analyzed in a specific way [9].

In addition, performance characteristics depend upon a coder used. Most coders are based on orthogonal transforms like DCT employed in JPEG or more advanced coders [10], wavelets [2] or Haar [11] transforms. Choice of compression technique is determined by many factors including priority of requirements as rate-distortion characteristics, simplicity of providing a desired quality or CR, computational efficiency, availability of DSP realizations or the corresponding platforms, etc. Concerning lossy compression of medical images, the so-called visually lossless compression is often required. This means that the introduced distortions should be invisible to enable image diagnostic value [1, 12].

In visually lossless compression, there are several important requirements to be satisfied. First, to be reliable, compression should be based on using adequate visual quality metrics and invisibity thresholds [13]. Second, a desired value of a used visual quality metric has to be provided quickly enough and with appropriate accuracy. Since in this paper, we consider grayscale images, it is possible to use PSNR-HVS-M [13] that is one of the most reliable visual quality metrics and which has a priori known threshold of distortion invisibility approximately equal to 42 dB [13]. Besides, as a particular case, we consider the coder AGU based on DCT [10] that performs better than JPEG and slightly better than JPEG2000.

There are several known ways to provide a desired quality of images compressed in a lossy manner. A universal approach is an iterative procedure [7] for which at each iteration the following is done: a) compression and decompression with a set value of parameter that controls compression (PCC) – this can be quantization step (QS) or quality factor or bpp (bits per pixel) depending upon a coder used; b) calculation of a used quality metric between original and compressed images; c) its comparison to a desired value of the used quality metric; d) decision undertaking to stop iterations or to change PCC with intention to make compression with providing the metric more close to the desired value. This procedure is able to provide quite accurate approaching to the desired quality of the compressed image but it has one essential drawback. The number of iterations is a priori unknown and, thus, it is unclear when compression will be completed.

Other approaches are based on metric prediction and PCC setting based on this prediction [14-16]. Some variants employ pre-established dependences of a given metric on PCC based on some approximation [16]. It might produce good results for certain range of PCC values but leads to quite large errors for other PCC values. Other methods [14] employ statistics determined for entire image for performance prediction but they are only slightly faster than compression/decompression and their accuracy of quality providing is worth improving. Recently, we have introduced a group of methods [14, 15] that obtain and "analyze" statistics in a limited number of blocks in DCT domain. However, these methods are mainly intended on prediction and providing of such quality metrics as MSE or PSNR that are known to be inadequate for visual quality of distorted images.

Therefore, in this paper, we propose to predict the metrics MSEHVSM used in calculation of the metric PSNR-HVS-M for the coder AGU. We demonstrate an opportunity to predict this visual quality metric analyzing only 500…1000 8x8 pixel blocks in DCT domain which is very fast. Accuracy of prediction and quality providing are studied.

II. Basic Dependences for Image Compression by AGU

The main idea of modern approaches to lossy image compression is that images can be sparsely represented by orthogonal transforms [1, 7]. The considered AGU coder belongs to DCT-based compression techniques. In opposite to the standard JPEG, AGU uses 32x32 pixel blocks, bit-plane coding of quantized DCT coefficients, and embedded deblocking after decompression. The parameter that controls compression is QS. With QS increasing, larger distortions are introduced and a larger CR is provided.

Let us examine compressed image quality using three quality metrics. One is standard PSNR and two other ones are PSNR-HVS and PSNR-HVS-M [13]. All three metrics are expressed in dB (the larger the better) and are defined similarly as

$$PSNR-HVS = 10log_{10}(255^2 / MSE_{HVS}) \quad (1)$$

$$PSNR-HVS-M = 10log_{10}(255^2 / MSE_{HVS-M}) \quad (2)$$

where MSE_{HVS} and MSE_{HVS-M} are specific MSEs calculated in DCT domain taking into account specific features of HVS. For PSNR-HVS, takes into consideration the known fact that distortions in low spatial frequencies are more visible than distortions in high spatial frequencies. For the metric PSNR-HVS-M, also takes into consideration the so-called masking effect (distortions in locally active areas as textures and edge/detail neighborhoods are less visible than distortions in homogeneous ones). PSNR, PSNR-HVS, and PSNR-HVS-M have equal values if distortions are like additive white Gaussian noise and masking effect is absent.

Consider the behavior of aforementioned quality metrics on QS. The dependences obtained for 512x512 pixel test image MRTprepared are presented in Fig. 1,a. Analysis of the plots allows concluding the following. For QS<7, all metrics are larger than 40 dB (PSNR-HVS-M exceeds 50 dB), this means that introduced distortions are invisible. In [15], the following approximation has been introduced for small QS:

$$MSE_{HVS-M}=0.02896\times QS^{1.976}. \quad (3)$$

The interval of larger QS (from 7 to approximately 30 that corresponds to from 1 to about 30, Fig. 2) relates to the most important practical cases. When QS increases, all metrics decrease (Fig. 1,a). PSNR-HVS becomes sufficiently smaller than PSNR for the same QS.

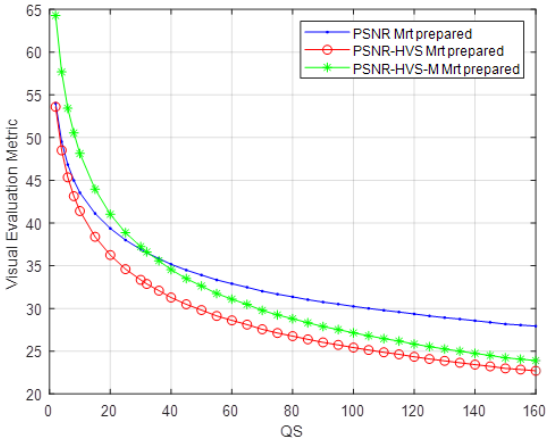

a

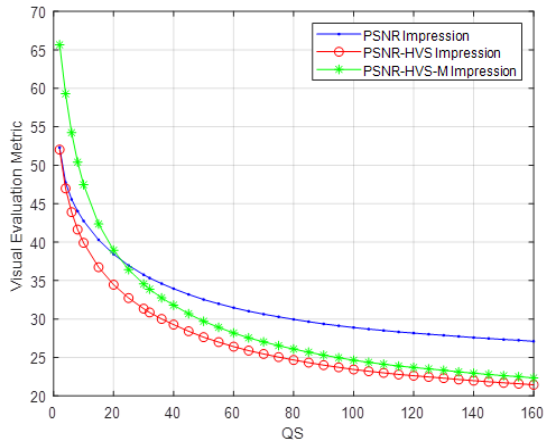

b

Fig. 1. Dependences of quality metrics on QS for two test images

This shows that introduced distortions are not like additive white Gaussian noise, more distortions are in low spatial frequencies. With further increasing of QS, PSNR-HVS-M also becomes smaller than PSNR. This shows that masking effect becomes small since distortions become too large. Meanwhile, PSNR-HVS-M are still larger than PSNR-HVS.

To check whether or not the behavior of dependences is the same for other images, the dental test image has been processed. The obtained dependences are given in Figure 1,b. Their comparison to the corresponding dependences in Fig. 1,a shows that they are very similar.

Fig. 2 taken from [15] with the fitted approximation curve [17] shows the scatter-plot for which each point corresponds to MSE_{HVS-M} determined for one test image compressed with a given QS. As it is seen, MSE_{HVS-M} values for the same QS can be quite different, especially for QS>30 where MSE_{HVS-M} values can differ by several times.

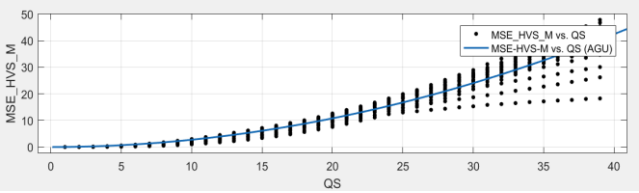

Fig. 2. Scatter-plot of MSEHVS-M on QS for lossy compression of grayscale images for the coder AGU

This means that prediction like (3) can lead to errors for particular images that can be too large and a more accurate prediction is needed. To solve this task, we have decided to come back to ideas in [12, 14] that presume using image statistics in a limited number of image blocks.

III. Prediction Based on Preliminary Analysis

Recall here that MSE_{HVS-M} is calculated as a mean value of local estimates of MSE_{HVS-M} in blocks (the number of such local estimates is about $I_{Im}J_{Im}/64$ where I_{Im} and J_{Im} define an image size. For traditional approach, all possible block positions have to be taken into account and MSE_{HVS-M} has to be calculated after image compression and decompression by a given coder.

In our case, we propose to calculate an estimate of MSE_{HVS-M} before compression using a limited number of blocks of size 8x8 pixels. Let us explain our intention. First, calculation of MSE_{HVS-M} is based on DCT and the coder AGU is based on 2D DCT as well although the block size is not 8x8 pixels. Because of this, we expect that there is correlation between MSE_{HVS-M} for AGU coder and MSE_{HVS-M} determined in a limited number of 8x8 pixel blocks (this hypothesis will be verified later). Second, DCT in 8x8 pixel blocks is a standard operation employed in image and video compression [18]. Thus, it has fast hardware and software realizations [19, 20]. Then, it is possible to expect that prediction can be carried out much faster than compression.

Thus, our idea is the following. Let us choose N 8x8 pixel blocks. Then, calculate 2D DCT for each block with getting D(k,l,n) where k=0,…7 and l=0,…7 are spatial frequency indices and n=1,…,N is a block index. After this carry out quantization for a given QS and determine

$$D_{dq}(k,l,n)=QS*([D(k,l,n)/QS]) \quad (4)$$

where [•] denotes rounding-off to the nearest integer. Then, $MSE_{HVS-M}(n)$ is calculated using Table of spatial frequency weights and masking rule (see [13] for more details). After this, average $MSE_{HVS-M\Sigma}$ is calculated for all blocks and MSE_{HVS-M_AGU} for AGU is predicted (the details of prediction are given blow).

Consider now some preliminary data showing that such a prediction is possible. Fig. 3 presents two examples of scatter-plots obtained for the test images Airfield and Goldhill. Color marks relate to estimates obtained in 8x8 pixel blocks while black marks relate to true values of MSE_{HVS-M_AGU} for AGU. QS varies from 1 to 100 with the step equal to 1.

Analysis of the presented scatter-plots and dependences shows the following:

1) MSEHVS-M_AGU increases when QS becomes larger, the dependence seems to be close to QS2, at least for small QS, although this should be checked more carefully;

2) Dependences of MSEHVS-M_AGU on QS seem to be very similar although the values for Airfield image are slightly larger than for Goldhill for the same QS (e.g., consider the case QS=80);

3) Values of MSEHVS-M_AGU seems to be mostly smaller than MSEHVS-MΣ for the same QS; then it comes an idea that some fixed correcting factor or correcting function (dependent on QS) can be used to recalculate an estimate MSEHVS-MΣ to an estimate of MSEHVS-M_AGU;

4) the estimates MSEHVS-MΣ behave in a rather compact manner where compactness of the estimates obtained for larger N is better; this means that N, as it can be expected, influences accuracy of prediction and this aspect has to be studied in more detail;

5) the diversity of the estimates MSEHVS-MΣ is the largest for N=100 (marked by green triangles) and the smallest for N=1000 (marked by purple rectangles).

Let us present the scatter-plots for two more typical test images, Baboon and Barbara where the former one is highly textural and the latter one is a middle complexity image (Fig. 4).

As one can see, the main dependences are the same. Properties of data for the test image Barbara (Fig. 4,b) are very similar to those for the test image Goldhill (Fig. 3,b) whilst the properies of data for the test image Baboon (Fig. 4,a) are more close to those one for the test image Airfield (Fig. 3,a) which is more textural as well.

Keeping in mind the aforementioned dependences, we have carried out the following statistical analysis for the considered set of test images. For each QS and each N, we have calculated mean and standard deviation of the ratio S = MSEHVS-MΣ / MSEHVS-M_AGU. The obtained data are presented in Fig. 5

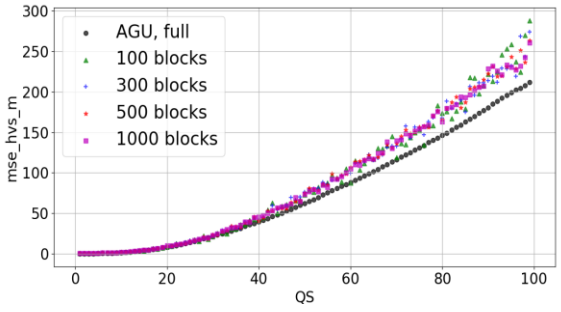

a

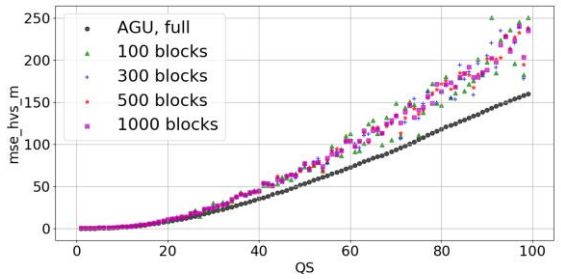

b

Fig. 3. Scatter-plots of estimates of MSEHVS-MΣ for different number of analyzed blocks and MSEHVS-M_AGU for images compressed by AGU for Airfield (a) and Goldhill (b) test images

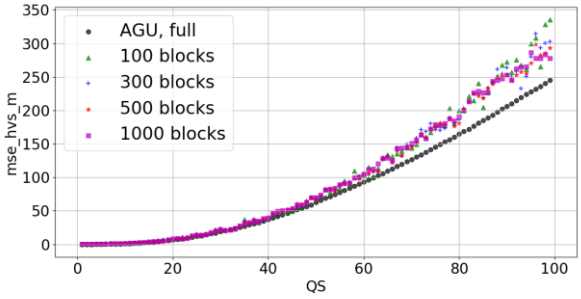

a

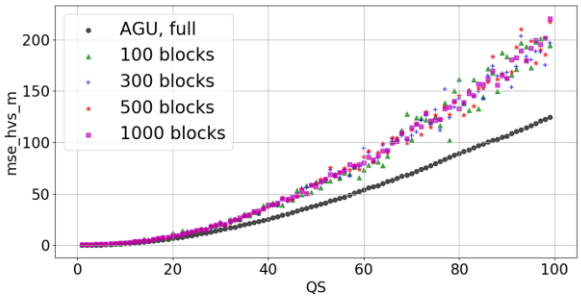

b

Fig. 4. Scatter-plots of estimates of MSEHVS-MΣ for different number of analyzed blocks and MSEHVS-M_AGU for images compressed by AGU for Baboon (a) and Barbara (b) test images

They are slightly surprising but interesting and useful. There is an interval of QS from 1 to approximately 7 where mean of S is quite large (considerably larger than unity) with an obvious tendency to decrease quickly. Standard deviation values are large in this interval too. This effects cannot be seen in Figures 3 and 4 since although the values of $MSE_{HVS\text{-}M\Sigma}$ are larger than $MSE_{HVS\text{-}M\_AGU}$, they are still very small. If QS>7, then the ratio has stable values close to 1.34. This ratio does not depend upon the number of analyzed blocks.

This means that the predicted $MSE_{HVS\text{-}M\_AGU}$ can be calculated easily as

$$MSE_{HVS\text{-}M\_pred} = MSE_{HVS\text{-}M\Sigma} / 1.34. \quad (5)$$

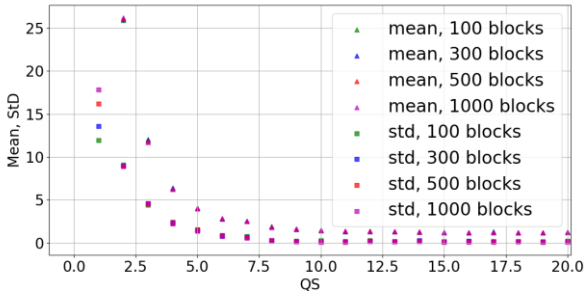

Fig. 5. Mean and standard deviations of the ratio MSEHVS-MΣ / MSEHVS-M_AGU for all test images compressed by AGU

So, now we have an algorithm for predicting MSEHVS-M_AGU. But, in practice, we need an algorithm to provide a desired MSEHVS-M_des. For this purpose, we propose to do the following:

1) calculate the initial value of quantization step QS as $QS_{init}=(MSE_{HVS\text{-}M}\ des/0.02896)^{1/2}$;

2) if $QS_{init} \leq 7$, use this QS_{init} as the final quantization step QS_{fin} for compression;

3) if $QS_{init} > 7$, then calculate $MSE_{HVS\text{-}M\Sigma}$ using a limited number of blocks and recalculate it to $MSE_{HVS\text{-}M\_AGU}$;

4) compare this $MSE_{HVS\text{-}M\_AGU}$ to $MSE_{HVS\text{-}M\ des}$; if accuracy is satisfactory (e.g., $MSE_{HVS\text{-}M\_AGU}$ differs from $MSE_{HVS\text{-}M\ des}$ by less than ε%, then use QS_{init} as QS_{fin}; otherwise determine QS_{fin} as

$$QS_{fin} = QS_{init} (MSE_{HVS\text{-}M\ des} / MSE_{HVS\text{-}M\_AGU})^{1/2} \quad (6)$$

where it is supposed that $MSE_{HVS\text{-}M\ AGU}$ is approximately proportional to QS^2.

IV. Verification Results

We have applied the proposed algorithm to all nine test images for two values of $MSE_{HVS\text{-}M\ des}$, namely equal to 4 that corresponds to invisibility of distortions and equal to 10 that relates to visible but not annoying distortions. The obtained data are presented in Tables 1 and 2, respectively.

As it follows from analysis of data in Table 1, $MSE_{HVS\text{-}M\Sigma}$ and $MSE_{HVS\text{-}M\_AGU}$ derived for QS_{init} are mostly considerably smaller than $MSE_{HVS\text{-}M\ des}$. This means that the approximation (3) is not quite accurate for small QS.

Thus, correction like (6) is needed. After correction, the provided MSE_{prov} is around $MSE_{HVS\text{-}M\ des}$, some values of MSE_{prov} are larger than $MSE_{HVS\text{-}M\ des}$ (this happens for complex structure images) and some are smaller (this takes place for simple structure images).

Note that CR values vary in very wide limits from 4…5 for complex structure images to almost 19 for simple structure ones.

TABLE I. DATA FOR MSEHVS-M DES=4

Image	QS_{init}	$MSE_{HVS-M\Sigma}$	MSE_{HVS-M_AGU}	QS_{fin}	MSE_{prov}	CR
aerial	12	2,014	1,503	20	6,195	5,75
airfield	12	2,431	1,814	18	6,129	4,26
baboon	12	2,041	1,523	19	5,769	4,50
barbara	12	3,653	2,726	15	3,505	8,70
Diego	12	1,840	1,373	20	6,790	4,50
frisco	12	4,314	3,220	13	3,482	18,5
goldhill	12	2,744	2,047	17	5,648	8,60
lenna	12	3,648	2,722	15	4,254	12,5
mrt	12	2,381	1,777	18	4,130	14,9

Consider now the data in Table 2. Again, $MSE_{HVS-M\Sigma}$ and MSE_{HVS-M_AGU} for QS_{init} are considerably smaller than $MSE_{HVS-M\ des}$. After correction, they become to be around $MSE_{HVS-M\ des}$ although some of them occur to be too large as for the test image Diego. Since more distortions are introduced, CR values have increased compared to data in Table I.

TABLE II. DATA FOR MSEHVS-M DES=10

Image	QS_{init}	$MSE_{HVS-M\Sigma}$	MSE_{HVS-M_AGU}	QS_{fin}	MSE_{prov}	CR
aerial	19	6,136	4,579	28	14,33	7,72
airfield	19	7,984	5,958	25	13,79	5,61
baboon	19	6,626	4,945	27	14,27	5,95
barbara	19	7,937	5,923	25	10,38	13,2
Diego	19	5,785	4,317	29	18,50	6,34
frisco	19	8,292	6,188	24	9,132	30,8
goldhill	19	9,066	6,765	23	11,24	12,1
lenna	19	8,949	6,678	23	8,909	19,2
mrt	19	6,126	4,572	28	10,82	21,2

Therefore, accuracy of providing $MSE_{HVS-M\ des}$ has increased compared to (3) but it is still worth improving. To our opinion, this can be done by evaluating compressed image complexity and taking this factor into account. Fig. 6 presents the test image MRT_prepared used in our analysis with the marked fragments that should be paid attention in analysis. The enlarged green frame fragment for compression with providing PSNR=38 dB is presented in Fig. 7a where introduced losses are invisible. The same fragment for compression with providing PSNR=36 dB is presented in Fig. 7b where introduced losses become noticeable.

This confirms that PSNR about 37 dB is the threshold of distortion visibility. Note that for the considered test image the coder AGU provides CR larger than JPEG by about 1.8 times. AGU also provides CR larger than JPEG2000 by about 1.2 times for PSNR from 30 to 40 dB. Equivalently, PSNR for AGU is sufficiently larger than for JPEG2000 or SPIHT [8] for the same CR.

Fig. 6. The test image MRT_prepared

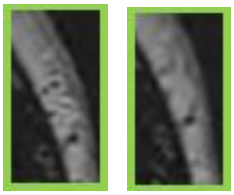

a b

Fig. 7. Fragments of compressed images

To partly prove this, Fig. 8 presents the dependences of the considered metrics on CR for the test image MRT_prepared for the coder AGU. Fig. 9 presents similar dependences for the compression technique SPIHT.

As one can see, all metrics decrease if CR increases. For CR about 10, introduced errors start to differ from additive white Gaussian noise (PSNR and PSNR-HVS start to differ considerably). For CR about 25, masking effect disappears (PSNR and PSNR-HVS-M become to be approximately the same).

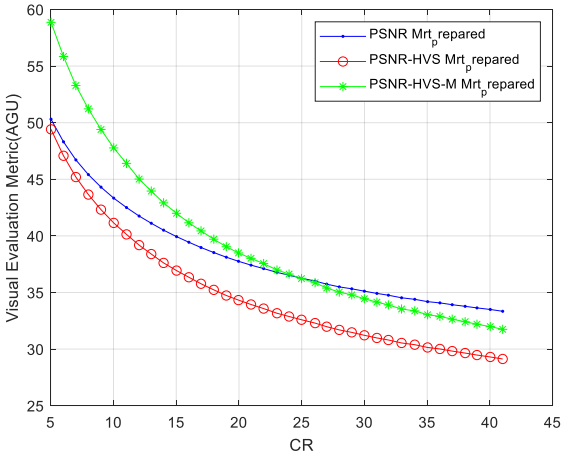

Fig. 8. Dependences of the considered metrics on CR for the test image MRT_prepared for the coder AGU

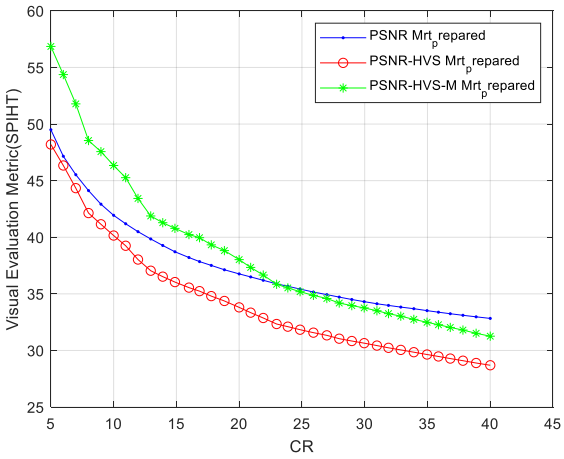

Fig. 9. Dependences of the considered metrics on CR for the test image MET_prepared for the coder AGU

Comparison of data in Figures 8 and 9 shows advantages of the coder AGU. The values of the corresponding metrics are 1…2 dB better (larger) than for SPIHT for the same compression ratio (for this purpose, compare the values of PSNR or PSNR-HVS-M for AGU and SPIHT in Figures 8 and 9, respectively, for CR≈20 that approximately corresponds to the case when distortions start to be visible to observers.

V. Conclusions

This paper analyzes peculiarities of lossy compression applied to medical and other types of images. It is demonstrated that the same QS or the same CR can correspond to essentially different visual quality of compressed images. If one needs to perform image lossy compression with providing a desired level of visual quality, visual quality metrics have to be used and their values have to be predicted.

We have shown that this can be done by simple and fast analysis of data in DCT domain for a limited number of image blocks (for example, 500 or 1000) chosen randomly. Such statistics allows incorporating image properties and to set PCC adaptively with respect to image complexity. We hope that the proposed approach can be applicable for other types of DCT-based coders.

References

[1] Stuart C. White, Michael J. Pharoah, Oral Radiology: Principles and Interpretation. Edition 7. Elsevier, 2014, 653 p.

[2] I. Blanes, E. Magli, J. Serra-Sagrista, “A Tutorial on Image Compression for Optical Space Imaging Systems”, IEEE Geoscience and Remote Sensing Magazine, 2(3), 2014, p. 8-26.

[3] Bairagi VK, Sapkal A. M: ROI-based DICOM image compression for telemedicine. Indian Acad Sci.2013;38(1):123–131.

[4] Advances in Medical Image Compression: Novel Schemes for Highly Efficient Storage, Transmission and on Demand Scalable Access for 3D and 4D Medical Imaging Data, University of British Columbia, 2010.

[5] David A. Koff, Harry Shulman, An Overview of Digital Compression of Medical Images: Can We Use Lossy Image Compression in Radiology? CARJ Vol 57, No 4, October 2006, pp. 211-217.

[6] Alexander C. Flint, Determining optimal medical image compression: psychometric and image distortion analysis, BMC Medical Imaging, 2012, 12:24, https://doi.org/10.1186/1471-2342-12-24

[7] A. Zemliachenko, N. Ponomarenko, V.Lukin, K. Egiazarian, J. Astola, Still Image/Video Frame Lossy Compression Providing a Desired Visual Quality, Multidimensional Systems and Signal Processing, June 2015, 22 p., DOI10.1007/s11045-015-0333-8

[8] D. Taubman, M. Marcellin, “JPEG2000 Image Compression Fundamentals, Standards and Practice,” Springer, Boston: Kluwer, 777 p., 2002, DOI: 10.1007/978-1-4615-0799-4.

[9] Al-Chaykh, O.K., Mersereau, R.M., “Lossy compression of noisy images”, IEEE Transactions on Image Processing, vol. 7, No 12, 1641-1652 (Dec. 1998).

[10] N.N. Ponomarenko, V.V. Lukin, K. Egiazarian, J. Astola, ”DCT Based High Quality Image Compression,” Proceedings of 14th Scandinavian Conference on Image Analysis, 14, 1177-1185, 2005.

[11] Minasyan S., Astola J., Guevorkian D., An image compression scheme based on parametric Haar-like transform. IEEE Int Symp Circ Syst. 2005;3:2088–2091.

[12] Krivenko S.S., Krylova O., Bataeva E., Lukin V.V., Smart Lossy Compression of Images Based on Distortion Prodection, Telecommunications and Radio Engineering, Vol. 77, No 17, 2018, pp. 1535-1554.

[13] V. Lukin, N. Ponomarenko, K. Egiazarian, J. Astola, Analysis of HVS-Metrics’ Properties Using Color Image Database TID2013, Proceedings of ACIVS, October 2015, Italy, pp. 613-624.

[14] R. Kozhemiakin, V. Lukin, B. Vozel, Image Quality Prediction for DCT-based Compression, Proceedings of CADSM 2017, Ukraine, February 2017, pp. 225-228.

[15] S. Krivenko, V. Lukin, B. Vozel, Prediction of Introduced Distortions Parameters in Lossy Image Compression, Proceedings of PICST, October 2018, Kharkov, Ukraine, 6 p.

[16] J. Minguillon, J. Pujol, "JPEG Standard Uniform Quantization Error Modeling with Applications to Sequential and Progressive Operation Modes", Electron. Imaging, 10(2), 2001, pp. 475-485.

[17] C. Cameron, A. Windmeijer, A.G. Frank, H. Gramajo, D.E. Cane, C. Khosla, “An R-squared measure of goodness of fit for some common nonlinear regression models,” Journal of Econometrics, 77(2), 16 p., 1997.

[18] https://www.springer.com/gp/book/9780792399988

[19] Tze-Yun Sung, Yaw-Shih Shieh, Chun-Wang Yu, Hsi-Chin Hsin. “High-Efficiency and Low-Power Architectures for 2-D DCT and IDCT Based on CORDIC Rotation”, Proceedings of the 7th ICPDC, 2006, pp. 191-196.

[20] https://www.math.cuhk.edu.hk/~lmlui/dct.pdf